Improved Accuracy of Amyloid PET Quantification with Adaptive Template–Based Anatomic Standardization

Yuma Tsubaki[1], Takayoshi Kitamura[2], Natsumi Shimokawa[1], Go Akamatsu[3], and Masayuki Sasaki[1]
for the Japanese Alzheimer's Disease Neuroimaging Initiative

[1]*Department of Health Sciences, Graduate School of Medical Sciences, Kyushu University, Fukuoka, Japan;* [2]*Department of Health Sciences, School of Medicine, Kyushu University, Fukuoka, Japan; and* [3]*National Institute of Radiological Sciences, National Institutes for Quantum and Radiological Science and Technology, Chiba, Japan*

Amyloid PET noninvasively visualizes amyloid-β accumulation in the brain. Visual binary reading is the standard method for interpreting amyloid PET, whereas objective quantitative evaluation is required in research and clinical trials. Anatomic standardization is important for quantitative analysis, and various standard templates are used for this purpose. To address the large differences in radioactivity distribution between amyloid-positive and amyloid-negative participants, an adaptive-template method has been proposed for the anatomic standardization of amyloid PET. In this study, we investigated the difference between the adaptive-template method and the single-template methods (use of a positive or a negative template) in amyloid PET quantitative evaluation, focusing on the accuracy in diagnosing Alzheimer's disease (AD). **Methods:** In total, 166 participants (58 healthy controls [HCs], 62 patients with mild cognitive impairment [MCI], and 46 patients with AD) who underwent ^{11}C-Pittsburgh compound B (^{11}C-PiB) PET through the Japanese Alzheimer's Disease Neuroimaging Initiative study were examined. For the anatomic standardization of ^{11}C-PiB PET images, we applied 3 methods: a positive-template–based method, a negative-template–based method, and an adaptive-template–based method. The positive template was created by averaging the PET images for 4 patients with AD and 7 patients with MCI. Conversely, the negative template was created by averaging the PET images for 8 HCs. In the adaptive-template–based method, either of the templates was used on the basis of the similarity (normalized cross-correlation [NCC]) between the individual standardized image and the corresponding template. An empiric PiB-prone region of interest was used to evaluate specific regions where amyloid-β accumulates. The reference region was the cerebellar cortex, and the evaluated regions were the posterior cingulate gyrus and precuneus and the frontal, lateral temporal, lateral parietal, and occipital lobes. The mean cortical SUV ratio (mcSUVR) was calculated for quantitative evaluation. **Results:** The NCCs of single-template–based methods (the positive template or negative template) showed a significant difference among the HC, MCI, and AD groups ($P < 0.05$), whereas the NCC of the adaptive-template–based method did not ($P > 0.05$). The mcSUVR exhibited significant differences among the HC, MCI, and AD groups with all methods ($P < 0.05$). The mcSUVR area under the curve by receiver operating characteristic analysis between the positive group (MCI and AD) and the HC group did not significantly differ among templates. With regard to diagnostic accuracy based on mcSUVR, the sensitivity of the negative-template–based and adaptive-template–based methods was superior to that of the positive-template–based method ($P < 0.05$); however, there was no significant difference in specificity between them. **Conclusion:** In quantitative evaluation of AD by amyloid PET, the adaptive-template–based anatomic standardization method had greater diagnostic accuracy than the single-template–based methods.

Key Words: Alzheimer's disease; amyloid PET; anatomic standardization; adaptive-template method

J Nucl Med Technol 2021; 49:256–261
DOI: 10.2967/jnmt.120.261701

Dementia is a brain disease showing disturbance of multiple higher cortical functions (*1*). The most common type of dementia is Alzheimer's disease (AD). It accounts for more than 50% of cases of primary disease causing dementia in Japan (*2*). The number of affected patients is expected to reach approximately 5.0 million by 2025 (*2,3*).

The cause of AD is thought to be neuronal degeneration induced by the accumulation of amyloid-β plaques and phosphorylated tau protein. Such an accumulation is considered to begin before the onset of cognitive impairment (*4*). Amyloid PET noninvasively visualizes amyloid-β plaques in the brain. The standard method of interpreting amyloid PET scans is visual binary reading, and objective quantitative evaluation is required in research and clinical trials. Anatomic standardization (i.e., spatial normalization) is essential for the quantitative evaluation of amyloid PET; for this process, a standard brain template is required. The standard templates are defined in the standard space (e.g., Montreal Neurologic Institute standard space), and various types of templates, such as an MRI T1-weighted template and an ^{18}F-FDG PET template, have been used for anatomic standardization (*5*). Although MRI-based methods are common for anatomic standardization of brain PET, PET-based methods have also been used in numerous studies for practical reasons (*6,7*). Amyloid PET demonstrates the activity distribution patterns that differ between amyloid-positive and amyloid-negative images. To account for the difference in activity distributions, Akamatsu et al. developed an adaptive-template–based method, which

Received Dec. 12, 2020; revision accepted Mar. 1, 2021.
For correspondence or reprints, contact Masayuki Sasaki (msasaki@hs.med.kyushu-u.ac.jp).
Published online April 5, 2021.

involves the use of multiple templates, both positive and negative (*8*). In the adaptive-template–based method, the template that is most similar to the subject image is selected and used for anatomic standardization. In some studies, the adaptive-template–based method has been used for amyloid PET anatomic standardization (*9,10*). However, the difference between the adaptive-template–based method and the single-template–based methods in amyloid PET quantitative evaluation has not been well elucidated.

In this study, the influence of the different anatomic standardization methods (the adaptive-template–based method and the single-template–based methods) on amyloid PET quantitative evaluation was investigated, focusing on diagnostic accuracy for AD.

MATERIALS AND METHODS

Participants

We retrospectively analyzed the data from 166 participants who underwent ^{11}C-Pittsburgh compound B (^{11}C-PiB) PET examination through the Japanese Alzheimer's Disease Neuroimaging Initiative (J-ADNI) study (*11*). The J-ADNI study is a multiinstitutional research project on AD led by the Ministry of Health, Labor, and Welfare and by the New Energy and Industrial Technology Development Organization in Japan. (*12*). The J-ADNI study was approved by the ethics committee of each institution for data acquisition, and written informed consent was obtained. The data used in this study were provided by the National Bioscience Database Center and were retrospectively analyzed. In addition, the requirement for written informed consent was waived. This study was approved by the ethics committee of Kyushu University, Fukuoka, Japan (approval 30-174).

All participants were native Japanese speakers, and their mean age was 70.5 ± 6.3 y (range, 60–84 y). The participants consisted of 58 healthy controls (HCs), 62 patients with mild cognitive impairment (MCI), and 46 patients with AD as shown in Table 1. The diagnoses of MCI and probable AD were based on the clinical criteria of the National Institute of Neurologic and Communicative Disorders and the Alzheimer's Disease and Related Disorders Association. The Mini-Mental State Examination–Japanese (MMSE-J), the Clinical Dementia Rating Scale–Japanese (CDR-J), and the Wechsler Memory Scale–R, Logical Memory II, corrected for education (WMS-R), were used to classify the early stages of dementia. The HCs scored 24–30 on the MMSE-J, 0 on the CDR-J, and above the cutoff on the WMS-R. The MCI patients scored 24–30 on the MMSE-J, 0.5 on the CDR-J, and below the cutoff on the WMS-R. The AD patients scored 20–26 on the MMSE-J, 0.5 or 1 on the CDR-J, and below the cutoff on the WMS-R.

TABLE 1
Participant Characteristics

Characteristic	HC	MCI	AD
Sex (*n*)			
Male	30	30	21
Female	28	32	25
Age (y)			
Mean ± SD	66.4 ± 4.5	71.4 ± 5.5	74.4 ± 6.3
Range	60–80	60–82	62–84
NINCDS-ADRDA	—	—	Probable AD
MMSE-J			
Mean ± SD	29.3 ± 1.1	26.7 ± 1.8	22.2 ± 1.8
Range	24–30	24–30	20–26
CDR-J	0	0.5	0.5 or 1.0
WMS-R	Above cutoff	Below cutoff	Below cutoff
Visually positive (*n*)	14	41	43
Visually negative (*n*)	44	21	3

NINCDS-ADRDA = National Institute of Neurologic and Communicative Disorders and Alzheimer's Disease and Related Disorders Association.

Imaging Protocol for ^{11}C-PiB PET

^{11}C-PiB PET was performed using 10 different PET camera models by 3 vendors as presented in Table 2 (*13*). PET images were reconstructed with data from 50 to 70 min after ^{11}C-PiB injection (555 ± 185 MBq). For attenuation correction, the segmented attenuation correction method by a 6-min transmission scan or a CT-based method was used, depending on scanner type, including stand-alone PET scanners and hybrid PET/CT scanners. Of the ^{11}C-PiB PET images, 88 were classified as visually positive, 68 as visually negative, and 10 as visually equivocal by 3 expert nuclear medicine physicians (*14*). All physicians had specialized in neuroimaging for more than 15 y. The results of the visual interpretation were based on the official judgment of the J-ADNI PET Core (*14*). In this study, the equivocal images were analyzed with the positive images (98 images).

Workflow of Quantitative Evaluation Method

The positive and negative templates were created in a previous study (*8*). Eleven typical positive images (4 AD and 7 MCI patients with high ^{11}C-PiB accumulation) were averaged to generate the positive template, and 8 typical negative images (8 HCs) were averaged to generate the negative template (*8*).

Figure 1 presents the workflow of the quantitative evaluation method (*8*). These processes were performed using the PMOD software, version 3.7 (PMOD Technologies LLC). First, the PET images were anatomically standardized to either the positive or the negative template. In the adaptive-template–based method, the PET images were standardized to both templates, and the template most similar to the subject image, according to the normalized cross-correlation (NCC), was selected. Second, the transformation vector of the anatomic standardization was recorded. Third, regions of interest were inversely transformed to individual PET images using a transformation vector. We calculated SUV ratio (SUVR) using the empirical PiB-prone region of interest, which was generated to evaluate regions where amyloid-β specifically accumulates (*8*).

The NCC was calculated to evaluate similarities between anatomically standardized images and the respective templates (*8*). In addition, the SUVR in 5 brain regions (posterior cingulate gyrus and precuneus, frontal lobe, lateral temporal lobe, lateral parietal lobe, and occipital lobe) was calculated; the reference region was the cerebellar cortex. The average SUVRs of the 5 regions were referred to as mean cortical SUVR (mcSUVR).

Statistical Analysis

JMP 13 (SAS Institute Inc.), was used for statistical analysis. The Steel–Dwass test was used to analyze the significance of differences between NCC and mcSUVR in the 3 groups (HC, MCI, and AD).

TABLE 2
PET Scanners and Reconstruction Parameters for ^{11}C-PiB PET in J-ADNI Study

Scanner vendor	Scanner model	Algorithm	Iterations	Subsets
GE Healthcare	Advance	Iterative (FORE + OSEM)	6	16
	Discovery ST Elite	Iterative (VUE Point plus)	2	40
Shimadzu	Eminence Sophia G/X	FORE + DRAMA	4	NA
	Eminence Sophia B/L	FORE + DRAMA	4	NA
	Eminence G/X	FORE + DRAMA	4	NA
	Headtome V	Iterative (FORE + OSEM)	4	16
Siemens	ECAT Accel	Iterative (FORE + OSEM)	6	16
	ECAT Exact HR+	Iterative (FORE + OSEM)	4	16
	Biograph 6	Iterative (FORE + OSEM)	4	16
	Biograph 16	Iterative (FORE + OSEM)	4	14

FORE = Fourier rebinning; OSEM = ordered-subsets expectation maximization; NA = not available; DRAMA = dynamic row-action maximum-likelihood algorithm.

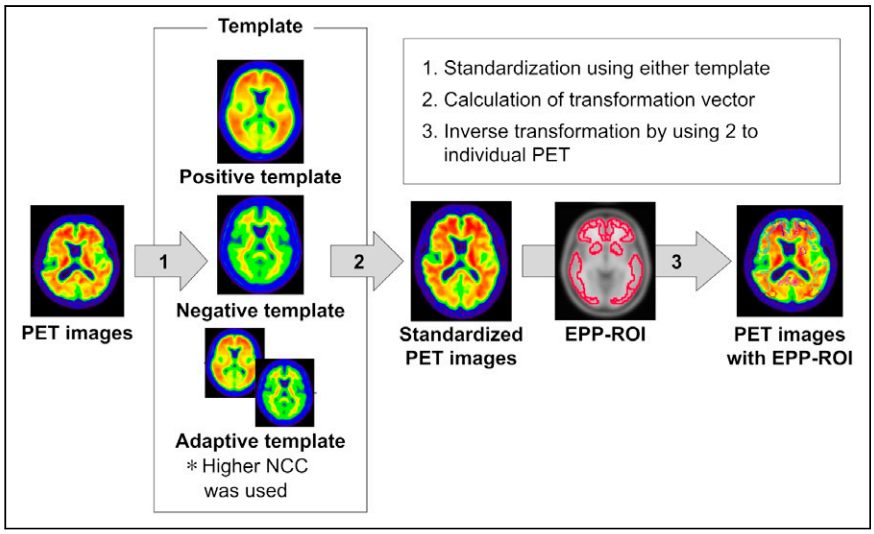

FIGURE 1. Workflow of PET-only quantitative evaluation method. First, PET images are anatomically standardized to either template using positive-template method, negative-template method, or adaptive-template method. Second, transformation vector used for standardization is calculated. Third, empirical PiB-prone region of interest (EPP-ROI) is inverse-transformed to individual PET image using transformation vector.

The McNemar test was used to analyze significance regarding diagnostic ability. The significance level was set to a P value of less than 0.05. The cutoff for differential diagnosis was obtained according to the method of maximizing Youden index (sensitivity + specificity – 1).

RESULTS

Concordance Rate Between Visual Evaluation and Used Template

Table 3 presents the concordance rate between the visual evaluation and the template that was used. When the adaptive template was used, the concordance of the adopted template with visual evaluation was 89.2%, and the association coefficient was 0.803.

NCC in Relation to Different Templates

The results of the NCCs are presented in Figure 2. When the negative template was used, the mean NCCs of the HC, MCI, and AD groups were 0.754 ± 0.122, 0.654 ± 0.143, and 0.580 ± 0.106, respectively. NCCs significantly differed among the 3 groups ($P < 0.05$). HCs who were visually negative had the highest NCC. When the positive template was used, the mean NCCs were 0.548 ± 0.130 for HCs, 0.701 ± 0.142 for MCI patients, and 0.777 ± 0.098 for AD patients. The results differed significantly among the 3 groups ($P < 0.05$): NCCs were higher for positive participants (MCI and AD) than for HCs. When the adaptive-template–based method was used, the mean NCCs were 0.778 ± 0.102 for HCs, 0.791 ± 0.072 for MCI patients, and 0.803 ± 0.050 for AD patients. All 3 groups exhibited high NCCs, which did not differ significantly.

The mcSUVR in Different Anatomic Standardization Methods

The mcSUVRs obtained using the different anatomic standardization methods are presented in Figure 3. When the positive template was used, mcSUVRs were 1.48 ± 0.33 for HCs, 1.86 ± 0.46 for MCI patients, and 2.12 ± 0.45 for AD patients. When the negative template was used, they were 1.35 ± 0.26 for HCs, 1.68 ± 0.42 for MCI patients, and 1.93 ± 0.44 for AD patients. On the other hand, the mcSUVRs of HCs, MCI patients, and AD patients were 1.37 ± 0.33, 1.80 ± 0.50, and 2.10 ± 0.47, respectively, when the adaptive template was used. The difference in mean mcSUVR among the 3 groups was greatest for the adaptive template. mcSUVR differed

TABLE 3
Visual Evaluation of Participants

Visual evaluation	Clinical diagnosis	No. of participants	No. of images		
			Positive template	Negative template	Adaptive template
Positive	HC	14	58	0	7
	MCI	41	62	0	35
	AD	43	46	0	38
	Total	98	166	0	80
Negative	HC	44	0	58	51
	MCI	21	0	62	27
	AD	3	0	46	8
	Total	68	0	166	86
Concordance rate			59.0%	41.0%	89.2%
Coefficient of association			not	not	0.80

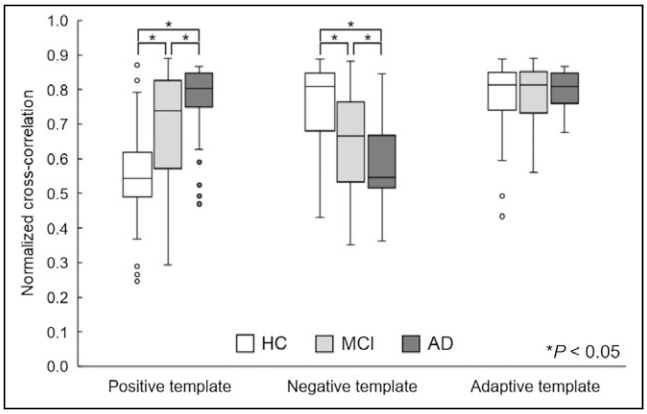

FIGURE 2. NCC results. *$P < 0.05$.

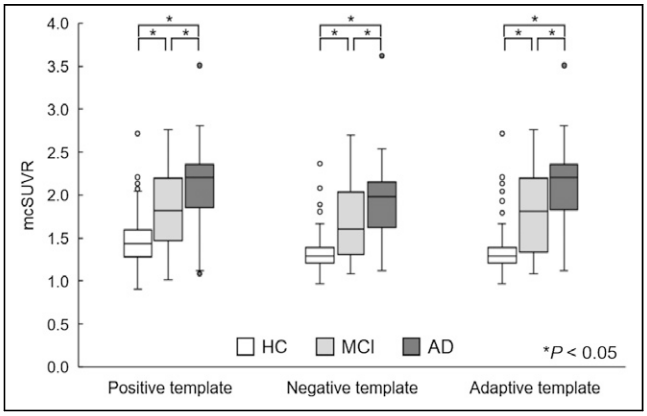

FIGURE 3. mcSUVR results. *$P < 0.05$.

significantly among groups for all methods ($P < 0.05$), although the difference was greatest when the adaptive-template–based method was used.

Diagnostic Ability in Different Anatomic Standardization Methods

Figure 4 and Table 4 show the results of receiver-operating-characteristic analysis for differentiating positive (MCI and AD) from negative (HC). The areas under the curve did not

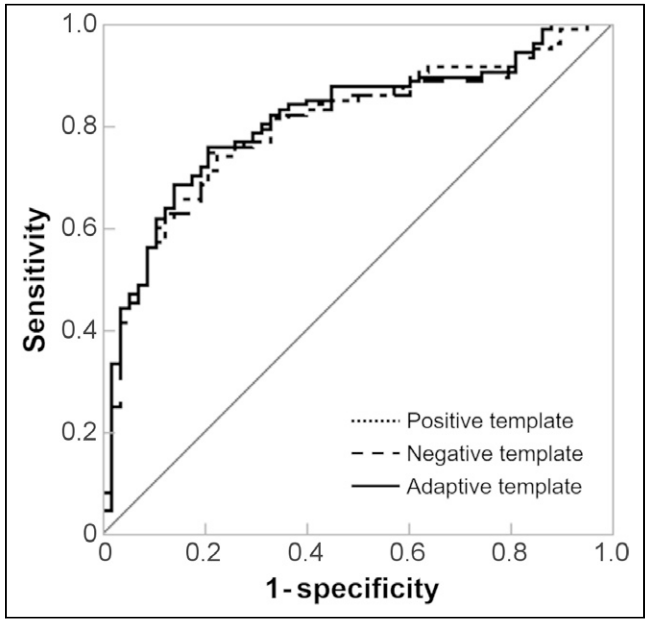

FIGURE 4. mcSUVR receiver-operating-characteristic curves for each template. Areas under curve for positive template–based method, negative template–based method, and adaptive template–based method were 0.806, 0.801, and 0.815, respectively.

significantly differ among the anatomic standardization methods; however, the area under the curve for the adaptive-template–based method was slightly larger than that for the single-template–based methods. The diagnostic ability of each method is presented in Table 4. The adaptive-template–based and negative-template–based methods exhibited significantly higher sensitivity than did the positive-template–based method ($P < 0.05$). Neither specificity nor accuracy differed significantly among methods; however, the accuracy of the adaptive-template–based method was the highest.

DISCUSSION

In this study, we examined the influence of the different anatomic standardization methods on ^{11}C-PiB PET

TABLE 4
Diagnostic Ability

Template	AUC	Cutoff	Sensitivity	Specificity	Accuracy
Positive	0.806	1.80	0.657	0.862	0.729
Negative	0.801	1.40	0.750*	0.793	0.765
Adaptive	0.815	1.40	0.759*	0.793	0.771

*$P < 0.05$ (difference from positive template).
AUC = area under curve.

quantitative evaluation, focusing on diagnostic accuracy for AD. The adaptive-template method was useful in improving the diagnostic performance of AD, as the mcSUVR difference among groups was greater with this method than with the single-template methods.

The adaptive-template method exhibited high agreement (89.2%) with visual classification. The mcSUVR of the HC, MCI, and AD groups differed significantly for all standardization methods. For the differential diagnosis, the adaptive-template–based method was most accurate.

The adaptive-template–based method exhibited higher NCCs in all groups than did the single-template–based methods. Lundqvist et al. and Bourgeat et al. examined ^{18}F-flutemetamol PET and ^{11}C-PiB PET, respectively (*9,10*). They reported that the template most similar to visual evaluation adopted by using a cross-correlation coefficient and normalized mutual information enhanced the quantitative accuracy. Therefore, the adaptive-template method is considered to be a successful adaptation of an individual PET image.

mcSUVR differed significantly among the 3 groups ($P < 0.05$), with the mcSUVR of the adaptive-template–based method being the largest (Fig. 3). For sensitivity and accuracy based on mcSUVR, the adaptive-template method outperformed the single-template methods. This improved performance is probably due to the fact that we calculated the cutoff to maximize accuracy. The negative and adaptive templates had the same cutoffs, whereas the positive template had a higher cutoff (Table 4). This cutoff (1.8) is high, compared with a previous study (1.5) (*15*), and may include a large number of false-negative cases (low sensitivity). The specificities of the templates did not differ significantly, although the specificity of the positive template was higher. The receiver-operating-characteristic curves did not significantly differ among the 3 methods, although the area under the curve for the adaptive-template–based method was superior to those for the single-template–based methods.

Edison et al. reported that the use of a conventional MRI-based template and a single PET template yielded comparable results in the ^{11}C-PiB PET quantitative analysis (*16*). Moreover, several studies have demonstrated that the use of multiple PET templates for anatomic standardization improved quantitative accuracy. Bourgeat et al. reported no significant difference between the SUVRs using the adaptive PET atlas approach and the MRI-based SUVR, although the SUVR obtained using the single mean PET atlas was significantly different from the MRI-based SUVR (*10*). Kang et al. developed a deep learning–based approach to generate multiple adaptive ^{11}C-PiB PET templates (*17*). This approach also significantly enhanced the quantitative accuracy of PET-based anatomic standardization (*17*). Our results suggested that the adaptive-template–based method can provide sufficient accuracy for amyloid PET anatomic standardization, although only 2 templates (positive and negative) were used.

This study had some limitations. First, the number of participants was small. Thus, further examination of a larger number of participants is needed to yield more robust results. Second, 2 templates were examined in this study. In the adaptive-template–based method, increasing the number of templates with various types of accumulation has the potential to improve the accuracy of anatomic standardization. Third, the PET data were acquired more than 10 y ago. Because recent PET scanners can provide higher-resolution images, the difference between positive and negative images might be clearer. Therefore, we expect the adaptive-template–based method to be effective for current PET images as well.

CONCLUSION

We have examined the influence of different anatomic standardization methods on amyloid PET quantitative evaluation, focusing on diagnostic accuracy for AD. The adaptive-template–based method slightly improved diagnostic accuracy in comparison with the single-template–based methods.

DISCLOSURE

This study was supported by JSPS KAKENHI grant 16K19882. No other potential conflict of interest relevant to this article was reported.

ACKNOWLEDGMENT

Data used in the preparation of this article were obtained from the J-ADNI database deposited in the National Bioscience Database Center (NBDC) Human Database, Japan (Research ID: hum0043.v1, 2016). As such, the investigators within J-ADNI contributed to the design and implementation of J-ADNI or provided data but did not participate in the analysis or writing of this report. A complete listing of J-ADNI investigators can be found at https://humandbs.biosciencedbc.jp/en/hum0043-v1.

REFERENCES

1. International statistical classification of diseases and related health problems. World Health Organization website. https://icd.who.int/browse11/l-m/en#/http%3a%2f%2fid.who.int%2ficd%2fentity%2f546689346. Updated May 2021. Accessed July 2, 2021.
2. Akatsu H, Takahashi M, Matsukawa N, et al. Subtype analysis of neuropathologically diagnosed patients in a Japanese geriatric hospital. *J Neurol Sci.* 2002;196:63–69.
3. Ninomiya T. Research on future projection of the population of the elderly with dementia in Japan [in Japanese]. Ministry of Health, Labour, and Welfare website. https://mhlw-grants.niph.go.jp/project/23685/1. Published 2015. Accessed July 9, 2021.

4. Jack CR Jr, Knopman DS, Jagust WJ, et al. Hypothetical model of dynamic biomarkers of the Alzheimer's pathological cascade. *Lancet Neurol.* 2010;9:119–128.
5. Evans AC, Janke AL, Collins DL, et al. Brain templates and atlases. *Neuroimage.* 2012;62:911–922.
6. Gispert JD, Pascau J, Reig S, et al. Influence of the normalization template on the outcome of statistical parametric mapping of PET scans. *Neuroimage.* 2003;19:601–612.
7. Della Rosa PA, Cerami C, Gallivanone F, et al. A standardized [^{18}F]-FDG-PET template for spatial normalization in statistical parametric mapping of dementia. *Neuroinformatics.* 2014;12:575–593.
8. Akamatsu G, Ikari Y, Ohnishi A, et al. Automated PET-only quantification of amyloid deposition with adaptive template and empirically pre-defined ROI. *Phys Med Biol.* 2016;61:5768–5780.
9. Lundqvist R, Lilja J, Thomas BA, et al. Implementation and validation of an adaptive template registration method for ^{18}F-flutemetamol imaging data. *J Nucl Med.* 2013;54:1472–1478.
10. Bourgeat P, Villemagne VL, Dore V, et al. Comparison of MR-less PiB SUVR quantification methods. *Neurobiol Aging.* 2015;36(suppl 1):S159–S166.
11. Shimokawa N, Akamatsu G, Kadosaki M, et al. Feasibility study of a PET-only amyloid quantification method: a comparison with visual interpretation. *Ann Nucl Med.* 2020;34:629–635.
12. Iwatsubo T. Japanese Alzheimer's Disease Neuroimaging Initiative: present status and future. *Alzheimers Dement.* 2010;6:297–299.
13. Ikari Y, Nishio T, Makishi Y, et al. Head motion evaluation and correction for PET scans with ^{18}F-FDG in the Japanese Alzheimer's disease neuroimaging initiative (J-ADNI) multi-center study. *Ann Nucl Med.* 2012;26:535–544.
14. Yamane T, Ishii K, Sakata M, et al. Inter-rater variability of visual interpretation and comparison with quantitative evaluation of ^{11}C-PiB PET amyloid images of the Japanese Alzheimer's Disease Neuroimaging Initiative (J-ADNI) multicenter study. *Eur J Nucl Med Mol Imaging.* 2017;44:850–857.
15. Jagust WJ, Bandy D, Chen K, et al. The Alzheimer's Disease Neuroimaging Initiative positron emission tomography core. *Alzheimers Dement.* 2010;6:221–229.
16. Edison P, Carter SF, Rinne JO, et al. Comparison of MRI based and PET template based approaches in the quantitative analysis of amyloid imaging with PIB-PET. *Neuroimage.* 2013;70:423–433.
17. Kang SK, Seo S, Shin SA, et al. Adaptive template generation for amyloid PET using a deep learning approach. *Hum Brain Mapp.* 2018;39:3769–3778.